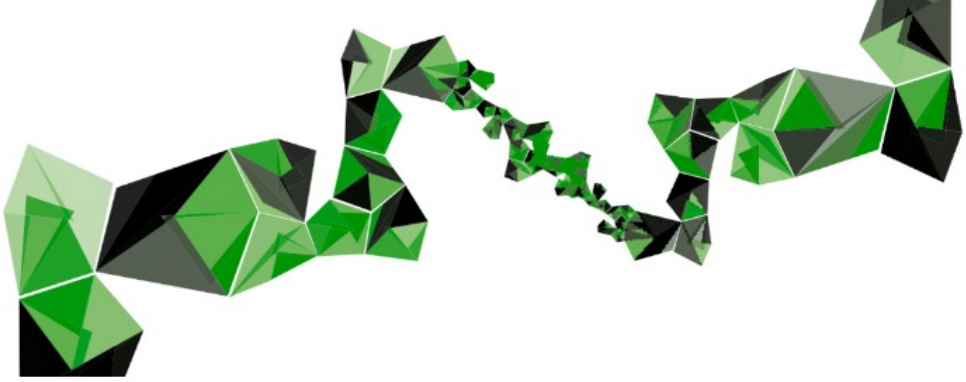

BACHELOR THESIS

Design of magnetically actuated rotational joint with a locking mechanism based on shape memory polymer for minimally invasive surgery.

Paula Kroon
s2737302

Faculty of Engineering Technology
Department of Biomedical Engineering

Examination Committee:
Chair: Prof. Dr. S. Misra
Daily Supervisor: MSc. S. Frieler
External Supervisor: Dr. I. Tamadon

1 July 2024

University of Twente

Abstract

Robotic manipulators are a growing field of research due to their ability to assist in minimally invasive surgery. Recently, magnetically-actuated robots have been proposed that are highly manoeuvrable to access hard-to-reach surgical sites. These robots, which are actuated by an externally applied magnetic field, consist of multiple joints which need to be able to shape-lock and unlock separately in order for the robot to move. This thesis is about the design of a mechanical locking mechanism to shape-lock the degree of freedom of a 360° rotational joint for an end-effector for minimally invasive surgery. The end-effector consists of a 3D printed shaft which can rotate with respect to an outer housing because of a permanent magnet attached to its tip placed in an external magnetic field. Ceramic ball-bearings allow the rotation while a locking-mechanism blocks this rotation. The locking mechanism consists of a lasercut locking ring and a 3D printed beam connected to the shaft. The beam made from shape memory polymer (SMP) has two states. A stiff state in which rotation of the shaft is shape-locked until at least a torque of 4.2 Nmm and a soft state stimulated by heat in which the SMP is flexible and deforms, allowing rotation from a torque of 0.859 Nmm. Finite element analysis and calculations determine the deflection of the beam in a stiff state at 0.0983 mm and in a soft state at 1.333 mm. The maximum bending stress in the beam in a stiff state is 33.94 N/mm^2 close to the yield strength of 40 MPa. Experiments in an electromagnetic coil setup confirm the locking mechanism shape-locks in a stiff state and rotates in a soft state. The design however has a backlash of 18 °in the locked state is a discrete locking mechanism.

Contents

List of Variables

Variable	Description	Unit
A	Cross-sectional area	m^2
B	Magnetic field strength	T
B_r	magnetic remanence	T
E	Elastic storage modulus	Pa
F	Force	N
I	Current	A
I_x	Moment of inertia	$k_g m^2$
L	Length	m
M	Moment	Nm
P	Power	W
R	Resistance	Ω
t	Thickness	m
T	Torque	Nm
T_g	Glass transition temperature	°C
T_{req}	Minimal required torque resistance	Nm
U	Voltage drop	V
V	Volume	m^3
w	Width	m
x	Distance	m
y	Deflection of the beam	m
y'	Angle of the beam	degrees
y''	Curvature of the beam	-
α	Angle between magnetic fields	degrees
$tan\delta$	Damping coefficient	-
μ	Magnetic moment	Am^2
μ_0	Permeability of vacuum	Hm^{-1}
ρ	Resistivity of the wire	Ωm
σ	Bending stress	Nm^{-2}
σ_{max}	Maximum bending stress	Nm^{-2}
σ_y	Yield strength	Nm^{-2}

1 Introduction

Minimally invasive surgery is a type of surgery where slender surgical tools, including a camera, are placed through small incisions in the body. A surgeon controls these instruments from outside the body while still being able to watch the procedure inside the body. The smaller incisions lead to a lower morbidity and shorter recovery period compared to conventional surgery [1, 2]. Currently the da Vinci robot is the most widely used surgical robot which lets a surgeon control the movement of each of the surgical tools remotely [3]. A downside of the laparoscopic instruments which are currently used however, is that the manoeuvrability of the laparoscopic tool is limited by a one-joint-movement [4] and they have difficulties to access hard-to-reach surgical sights.

Magnetically-actuated surgical devices are a growing field of research to assist in minimally invasive surgery due to the possibility of contactless steering [5]. Specifically magnetically-actuated manipulators have been proposed to be highly maneuverable and compact, which allows them to access hard-to-reach surgical sights in the body. By locking individual joints or segments, the manipulator can be controlled by an externally applied magnetic field and a single permanent magnet at its tip [6]. To be able to control all joints separately, each joint needs a locking mechanism. Plooi et al (2015) described multiple locking mechanisms based on mechanical locking like a ratchet with gear and pall, but also friction based locking mechanisms [7]. One of these friction based locking mechanisms is the thermic lock where a heated material expands and creates friction. Peerdeman et al (2014) designed a hand prothesis where the fingerjoints are activated and deactivated with friction locking [8]. There are several magnetic surgical devices that use shape-memory polymers (SMPs) [6]. SMP is a polymer which can become flexible and change shape when stimulated [9]. Yang et al (2016) designed a locking mechanism for a ball joint based on a shape-memory polymer [10]. A socket and ball are separated by a layer of SMP. While the SMP is soft, the ball is able to rotate inside its socket. When the SMP is stiff, the ball and socket are mechanically locked and therefor the joint can not rotate.

For surgical procedures, a rotational degree of freedom (DOF) is inevitable. Procedures that involve gripping, dissection or drilling require a rotational DOF that can be locked at any desired position. To the best of our knowledge, no work has been done on a magnetically-actuated 360° rotational joint based on shape-memory polymers. Therefor, this thesis is about the design of a shape-memory polymer based locking mechanism to shape-lock the degree of freedom of a 360° bi-directional, rotational joint. This rotational joint has the potential to serve as an end-effector on a magnetically-actuated surgical instrument, while adding a rotational DOF to the system.

2 Theoretical Background

2.1 Shape-Memory Polymers

Shape-memory polymers (SMPs) are smart materials which can change shape when stimulated and have a memory effect [9, 11, 12]. SMPs can be in a stiff, glassy state or a soft, rubbery state with a transition state in between [13]. During the synthesising of SMP, polymer chains cross-link to form into an original state. Stimuli like heat, electricity, moisture or magnetism allows the SMP to transition from glassy state to the rubbery state in which the SMP is able to deformed [9, 11, 12]. When the stimuli is removed, the SMP stays in a temporary state until it is stimulated again. The memory effect ensures that the SMP goes back to its original state when the SMP is stimulated without external forces acting on the material [13].

The most common type of SMP is the thermo-actuated SMP [13]. The transition state gets activated when the material is heated above glass transition temperature (T_g). The transition temperature can be reached by internal and external heating. A dynamic mechanical analysis (DMA) is used to determine the transition

temperature of the sample. During a DMA is a sinusoidal stress applied on the sample material which results in sinusoidal deforming. The phase shift as a result of the viscoelastic behaviour of the material is the damping factor tan δ [14]. The peak of the tan δ shows the transition temperature [15]. Figure 1 shows the results of a DMA where the state of the material can be divided into regions. The elastic storage modulus shown as a red line in the figure shows the stiffness of the material while the temperature increases. In the glassy region, at a low temperature, the sample has a high and constant elastic storage modulus and the material is stiff. In the glass transition region is a strong decrease in the elastic storage modulus and a peak of tan δ which gives the transition temperature. In the rubbery state, at a lower constant storage modulus, the sample is elastic and can deform [16].

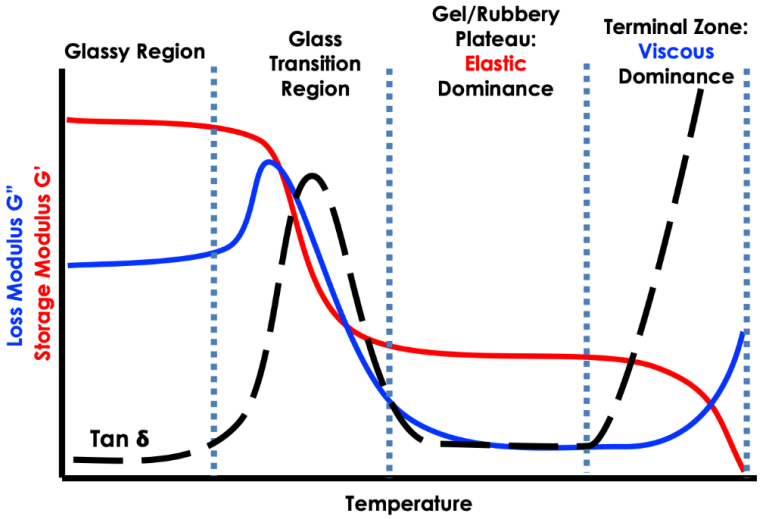

Figure 1: *Dynamic mechanical analysis result showing the different states of the sample. The red line shows the elastic storage modulus in each state. The black striped line shows the tangent δ where the peak in the glass transition region corresponds with the transition temperature of the material [17].*

2.2 Locking Mechanisms

The locking and unlocking of relative movement between two parts can be achieved by various locking mechanisms. Rotational locking mechanisms, which are used in this report, lock and unlock an inner ring rotating with respect to an outer ring [7].

Mechanical locking is when one part obstructs the movement of another part for example in latches and ratchets. A latch uses a pawl and a hook where one is able to move and therefor shape-lock with the other. Latches can have one hook or multiple hooks on a linear or circular rotating structure where the pawl can shape-lock. Both active and passive shape-locking is possible, where passive shape-locking happens because of the velocity or position of the components. Ratchets have a pivoting pawl which interacts with a gear. A passive way of the pawl engaging with the gear is by a spring which allows one direction of rotation only. An active way of the pawl shape-locking on the gear is by compression or tension on the pawl. Often mechanical locking mechanisms have discrete locking [7].

Friction-based locking uses friction between parts to prevent relative motion. Friction based locking is often continuous locking. However, it has a limited locking torque. Examples of friction-based locking mechanisms are overrunning clutches and thermic locking. An overrunning clutch has similar to ball-bearings an inner and an outer ring moving with respect to each other because of rolling elements. If the mechanism locks is determined by the rotational speed. A thermic lock uses the properties of a material that expands when heated. A first part rotates compared to a second part. However, the expanded material creates friction

during rotation and therefor locks the joint under specific force [7].

2.3 Magnetic Actuation

Magnetically actuated manipulators rely on magnetic fields for the movement of the manipulator. Magnetic fields are generated by either a permanent magnet of electromagnets. A magnet consists of a north and a south pole with field lines flowing from north to south as shown in Figure 2.

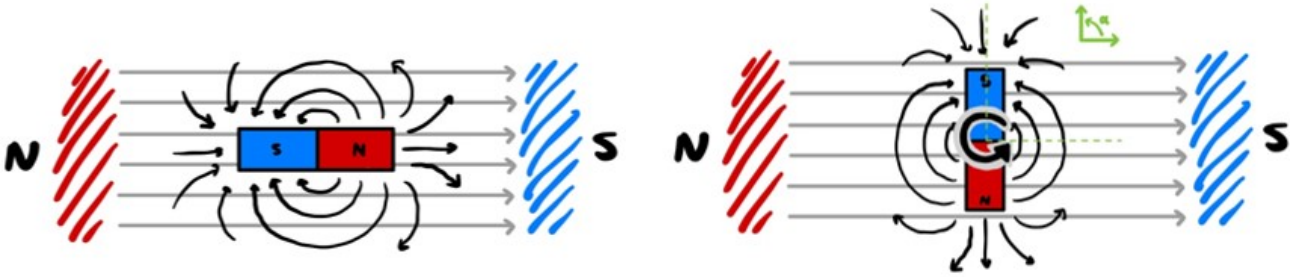

(a) **(b)**

Figure 2: *A permanent magnet placed in an external field tries to align with the field lines.* **(a)** *A magnet is aligned with an external field and therefor no torque is exerted onto the permanent magnet.* **(b)** *A magnet is rotated 90°with respect to the external magnetic field which exerts a maximum torque on the permanent magnet.*

Magnetic field lines from multiple fields will always try to align with each other. Therefor two opposite poles will always attract each other while two poles of the same polarity will repel from each other. In Figure 2a is the permanent magnet perfectly aligned with the external field with angle α equal to zero. In Figure 2b is the magnet 90 °rotated compared to the external field and therefor a torque is generated to align the fields. The torque is maximum at 90°and zero at 0°. A Torque generated by a magnetic field is given by

$$T = \mu B sin(\alpha) \tag{1}$$

where B is the strength of the external magnetic field in Tesla, α is the angle between the external magnetic field and the permanent magnet and μ is the magnetic moment given by

$$\mu = \frac{B_r V}{\mu_0} \tag{2}$$

with V the volume of the magnet, B_r the magnetic remanence of the magnet and μ_0 the permeability of vacuum equal to $4\pi \cdot 10^{-7}\ Hm^{-1}$.

A permanent magnet can be made from multiple materials and in different types. Materials which are used include magnetic materials like Iron, Nickel, Cobalt, Gadolinium and Dysprosium [18]. Types of magnets include disc magnets, ring magnets, block magnets and U-shaped magnets. These magnets can be axially magnetised or diametrically magnetised. This report focuses on diametrically magnetised ring magnets.

Moving electrical charge is next to permanent magnets also able to generate a magnetic field. The magnetic field generated by a straight wire is circular around the wire, while coiling a magnet generates a linear magnetic field inside the coil. Increasing the amount of coils increases the magnetic field strength. A homogeneous magnetic field can be generated using a Helmholtz coil configuration. Three pairs of coils are placed orthogonal to each other. The distance between the coils equals the radius of the coil [19].

2.4 Euler-Bernoulli Beam Theory

Euler-Bernoulli's beam theory describes the deflection of a beam by a force or moment acting on the beam. Assumed is that the deflection in the beam is very small. A second assumption is that the material is homogeneous and does not experience permanent deformation. Therefor the stress-strain relation is linear. The curvature in the beam can be described by

$$\frac{d^2y}{dx^2} = -\frac{M(x)}{EI_x} \tag{3}$$

where y is the deflection in the beam at distance x from the fixed end of the beam and $M(x)$ is the moment acting on the beam which results in a deflection [20]. E is the elastic storage modulus of the material of the beam and I_x is the moment of inertia given by

$$I_x = \frac{wt^3}{12} \tag{4}$$

in the case of a rectangular beam where w is the width of the beam and t the thickness [20].

Figure 3 shows a beam with length L, fixed in point A with a force F acting on point B, resulting in a deflection. The horizontal and vertical force and the moment in point A can be determined by

$$\sum F_x = A_x = 0 \tag{5}$$

$$\sum F_y = A_y - F = 0 \tag{6}$$

$$\sum M = -M_A - F \cdot L = 0 \tag{7}$$

since the sum of all forces and moments acting on a body equal zero.

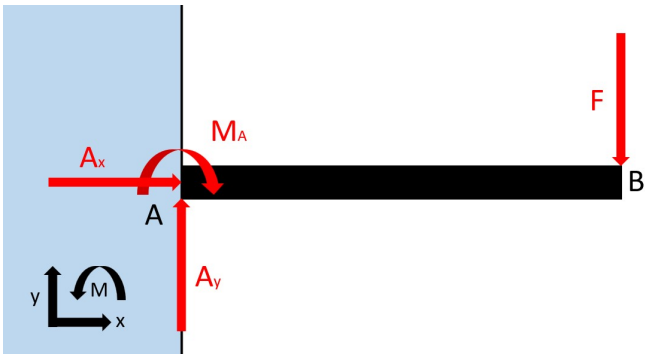

Figure 3: *A beam fixed in A with force F acting on B.*

The moment acting at point x somewhere between A and B, is determined by $\sum M = 0$ and is given by

$$M(x) = M_A + A_y \cdot x \tag{8}$$

where x is the distance from point A to the point on the beam. Implementing this equation in Equation 3 gives

$$E \cdot I_x \cdot y''(x) = -A_y \cdot x - M_A \tag{9}$$

where $y''(x)$ is the curvature of the beam. Integrating this equation gives the angle in the beam $y'(x)$ by

$$E \cdot I_x \cdot y'(x) = -\frac{1}{2}A_y \cdot x^2 - M_A \cdot x + C_1 \tag{10}$$

and the deflection $y(x)$ by

$$E \cdot I_x \cdot y(x) = -\frac{1}{6} A_y \cdot x^3 - \frac{1}{2} M_A \cdot x^2 + C_1 \cdot x + C_2 \tag{11}$$

where C_1 and C_2 are two constants. The boundary conditions at point A of the beam are $y(x = 0) = 0$ and $y'(x = 0) = 0$. Implementing these boundary conditions give the unknown constants $C_1 = 0$ and $C_2 = 0$. At point B of the beam is the length x equal to L. Implementing Equations 6, 7 and the constants C_1 and C_2 leads to the equation for the deflection y given by

$$y = \frac{FL^3}{3EI_x} \tag{12}$$

where F is the force acting on the tip of the beam, L is the length, I_x is the moment of inertia and E is the elastic storage modulus of the material of the beam.

The moment acting on the beam also leads to bending stress in the beam. The bending stress σ increases the further away from the neutral line with a maximum bending stress σ_{max} at the edge of the beam. In a rectangular beam is the neutral line in the middle of the beam. The maximum bending stress is given by

$$\sigma_{max} = \frac{My_{max}}{I_x} \tag{13}$$

where y_{max} is the distance between the neutral line and the top or bottom of the beam [20].

The stress and strain in a material have a linear relation until a yield point. After this point the strain of the material increases faster compared to the stress which eventually results in breaking of the material. When the bending stress in the material stays below the yield strength σ_y, there is no permanent deformation [20].

2.5 Joule Heating

Joule heating is a method of actively generating heat via a wire. The resistance in the wire can be determined by

$$R = \rho \cdot \frac{L}{A} \tag{14}$$

where ρ is the resistivity of the wire, L is the length and A is the cross-section of the wire [21]. Ohm's law which is given by

$$U = R \cdot I \tag{15}$$

gives the relation between the current I running through, the voltage drop V over and the resistance R of the wire. The power output is given by

$$P = U \cdot I \tag{16}$$

where a higher power output generates more heat [21].

3 Methods

3.1 Requirements

This thesis is about the design of an end-effector with a locking mechanism for a rotational joint. The rotational motion is actuated by an external magnetic field, which means a permanent magnet is attached to the end-effector. The end-effector should be made from a material which does not interact with the magnetic fields. The design should allow bi-directional rotation in an unlocked state. The magnetic field strength required for rotating should not exceed 55 mT, as this is the maximum field strength of the magnetic actuation system used. The design should also shape-lock the rotational motion when needed. In this

state, the locking mechanism should withstand a minimal required torque T_{req} of 4.0 Nmm. The locking mechanism should be continuous meaning the design should shape-lock at all 360° of rotation. This is necessary for allowing surgical tools to be held in place at any required angle.

The end-effector with locking mechanism should have an outer diameter of 9-15 mm which is a typical range for endoscopes for the digestive tracts [22] and making it a compact design. A hollow tube through the design is needed for a working channel for surgical tools.

3.2 Concept Design

The concepts made for this thesis consist of an inner shaft rotating with respect to an outer housing and a locking mechanism blocking this relative motion. The general concept of the end-effector is shown in Figure 4. A diametrically magnetised ring magnet (colored blue/red) attached to the shaft (colored in pink) ensures the rotation of the pink shaft. An external magnetic field is applied on the end-effector resulting in the poles of the magnet aligning with the external field. An external rotating field ensures the permanent magnet and the connected shaft to rotate with the field. The ball-bearings (colored in green) allow the rotation of the shaft while keeping the shaft aligned with the housing. The general idea is that the locking mechanism (represented as a yellow ring) blocks this relative rotation by shape-locking the outer housing to the inner shaft. The locking mechanism consists of a shape-memory polymer. In a locked state is the shaft shape-locked to the outer housing and therefor blocks the rotational motion. In an unlocked state is the SMP flexible which allows rotation of the shaft with respect to the outer housing. For this design to be used for surgical applications, a working channel is needed inside the shaft where surgical instruments go through.

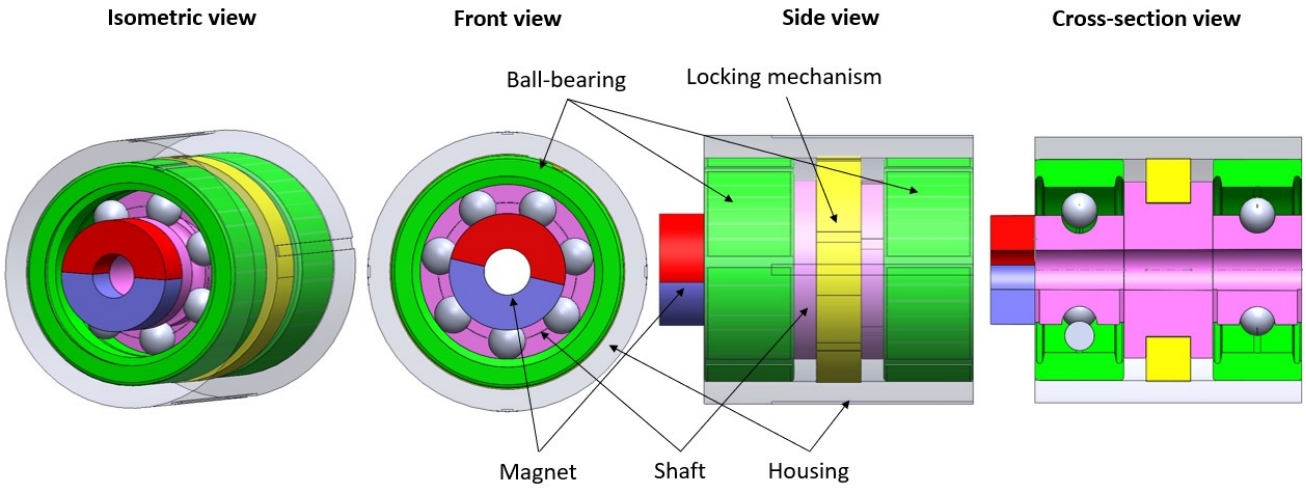

Figure 4: *General concept of the end-effector with locking mechanism. The ball-bearings connect the shaft to the outer housing while allowing rotation. The diametrically magnetised actuates the rotation of the shaft while the locking mechanism blocks rotation.*

Multiple concepts are designed which differ in the locking mechanism. The concepts are described in Appendix A. The final design has a locking mechanism based on beam deflection. The design can be seen in Figure 5a. It consists of a locking ring (colored yellow) with multiple dents and is connected to the outer ring of the ball-bearing. The shaft shown in pink can rotate with respect to the locking ring and outer housing when a magnetic field is applied. The beam (colored orange) can block this rotation. The beam is made from a shape-memory polymer which enables the material to be both stiff and flexible depending on its temperature. In the locked position is the beam stiff and shape-locks between two dents on

the locking ring. When the beam is soft, the rotation of the shaft will make the beam deflect around a dent allowing the rotational motion. The magnet attached to the shaft rotates with the external field as long as the beam is flexible. The memory property of the SMP ensures the beam straightens in the next dent.

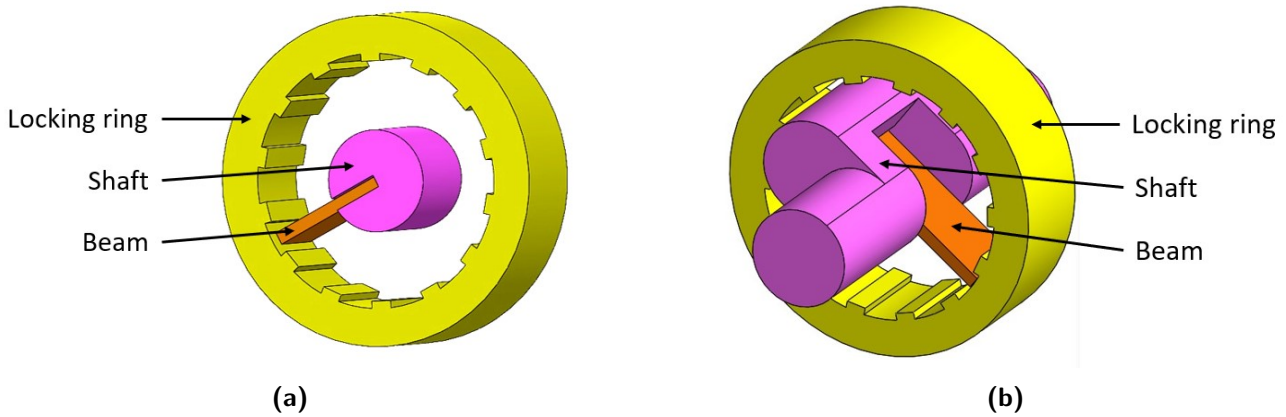

Figure 5: *Locking mechanisms based on a deflecting beam with variable stiffness. The SMP beam shown in orange is connected to the shaft and engages with the outer ring. In the stiff state, the beam shape-locks the rotation. In the soft state, it enables rotation.* **(a)** *A beam is connected to a straight shaft. This design is tested in this thesis.* **(b)** *A conceptual design of a locking mechanism with a U-shaped shaft to increase the length of the beam.*

In this concept one beam is used for shape-locking on the locking ring. Other designs could include more beams connected to the shaft. This increases the torsional stiffness of the design, however also more torque is required for rotating if the beams are in a flexible state.

To reduce the bending stress, the length of the beam can also be increased. This can be done by using a 'U' shape in the shaft at the location of the locking mechanism, where the beam is connected to the bottom of the 'U'. This can be seen in Figure 5b. Increasing the length reduces the torque required for rotating in a flexible state, however it also reduces the torsional stiffness in a stiff state.

3.3 Materials

The end-effector is actuated by a magnet. A diametrically magnetised magnet is used to make rotation possible. The ring magnet is made from NdFeB and has a coating from Ni-Cu-Ni. The magnet has a magnetisation of N45 which equals to a magnetic remanence B_r of 1.350 T [23]. With outer and inner diameter equal to 10 and 5 mm respectively and a height of 5 mm, the volume V of the magnet is equal to 0.2945 cm^3.

The ball-bearings consist of multiple materials which do not interact with the magnetic field. The rolling elements in the ball-bearings are made from glass, the cage is from polyamide and the inner and outer housing of the ball-bearings are from polyoxymethylen. The dynamic load rate of the ball-bearing is 35 N. The ball-bearings have an outer diameter of 13 mm, an inner diameter of 4 mm and a thickness of 5 mm. [24]

The outer ring of the locking mechanism shown in yellow in Figure 5 is lasercut from a Polymethylmethacrylaat (PMMA) sheet. The outer diameter of the locking mechanism is set at 13 mm to match the dimensions of ball-bearings. The wall-thickness of the ring is limited by the lasercutter due to heat morphing to accuratly cut the design at minimally 3 mm. Therefor the inner diameter is 10 mm with the dents pointing inwards.

The shaft and the beam are both is 3D printed. The shaft is made from Acrylonitrile Butadiene Styrene (ABS), while the beam is printed from black polylactic acid (PLA) with a yield strength σ_y of 40MPa [25]. A DMA-measurement is done to determine the thermo-mechanical properties of the PLA beam, like the transition temperature and the elastic storage modulus in the two states. To actively heat the beam, Joule heating is used. This is done by attaching two thin layers of PLA to each other with heating wires in between. The wall thickness of one of these layers is 0.25 mm. Attaching two layers creates a 0.5 mm thick beam. The heating wires are made from stainless steel with a resistivity of 0.72 $\cdot 10^{-6} \Omega m$ [26].

3.4 Concept Testing

The design made with said materials can be tested to validate whether it meets the requirements. A DMA-measurement determines the transition temperature from glassy to rubber-like state. With the same test, the modulus of elasticity of the materials in each of the states can be determined. With these values for the elastic storage modulus, the width of the beam w can be determined with equation 12. The width is determined for a beam with a length of 2.9 mm in a stiff state.

The transition temperature in the beam can be reached with Joule heating. The current required for reaching the transition temperature can be determined by evaluating the temperature curve at multiple currents. This is done using a thermal camera. The voltage is set at 5 Volts while different measurements with different currents are done varying from 0.1 to 0.3 Amperes. The measurements starts at the same time the joules heating starts. The Joule heating ends when the temperature saturates at a maximum value. The measurement stops when the temperature of the beam is back at starting temperature. The current of which the maximum temperature corresponds with the transition temperature is used for testing the design.

The locking properties of the locking-mechanism can be determined using a electromagnetic coils and applying a current. The setup used is the electromagnetic coil setup PaCMag, an approximation of the Helmholtz coil configuration. 3 Pairs of coils are placed orthogonal to each other. The end-effector with locking mechanism is placed inside the centre of PaCMag.

The locking of the rotational joint can be tested with the beam in glassy state. In this case no Joule heating is required. A current in the coils with the axis perpendicular to the magnetic field of the permanent magnet attached to the shaft is applied to maximize the torque on the shaft. The magnetic field in one direction is increased to determine at what magnetic field and therefor at what torque the locking mechanism holds. This can be calculated using Equation 1. The deflection of the beam and the maximum bending stress are calculated with Equations 12 and 13. A finite element analysis for both the deflection and the bending stress is also done.

The backlash can be determined in this setup. This is done by rotating the beam in locked state maximally in one direction and determining the angle of the beam. The same is done for the other direction. Determining the difference between angles gives the freedom of the beam in locked state, in other words, the backlash.

To determine what torque is required for rotating the shaft in an unlocked state, the same setup can be used. In this scenario the beam is heated above the transition temperature for the beam to become soft. The magnetic field is increased until the beam bends enough until it slips to a next dent. The torque corresponding to this magnetic field is calculated with Equation 1. Due to the beam theory only holding for small deflections, A finite element analysis is done for determining the deflection and the bending stress.

4 Results

4.1 Dynamic Mechanical Analysis

To determine the thermo-mechanical properties of a PLA sample, a dynamic mechanical analysis is done. Figure 6 shows the elastic storage modulus plotted against the temperature. The shape-memory polymer changes from glassy state to transition temperature range state into rubbery state where the glass transition temperature at the highest value of tangent δ is at 64 °C. The elastic storage modulus when the SMP is cold in glassy state at 30°C is 3.87 GPa. The storage modulus of the beam in a soft rubbery state is determined based on the exact temperature of the beam after heating which is described in Chapter 4.3.

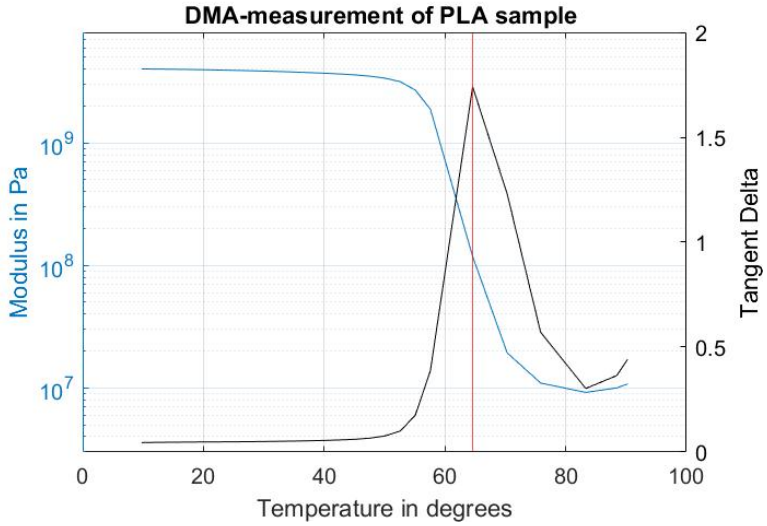

Figure 6: *DMA plot with elastic storage modulus plotted on the left axis against Temperature [°C] and the tangent δ plotted on the right axis in black. The blue line shows the elastic storage modulus at increasing temperature. The glass transition temperature in red is at 64 °C.*

4.2 Design

The final design as described in Chapter 3.2 can be seen in Figure 7. The magnet is the tip of the end-effector which is fixed to the shaft. The shaft runs through the entire design and is connected to the inner rings of the two ball-bearings. In between the ball-bearings there is space for a locking ring with 14 dents for shape-locking. The outer diameter of the design is 13 mm. The beam which is fixed to the shaft, shape-locks on the dents of the locking ring. Heating wires are connected to the beam to enable the beam to become flexible. The design of the beam can be seen in Figure 8.

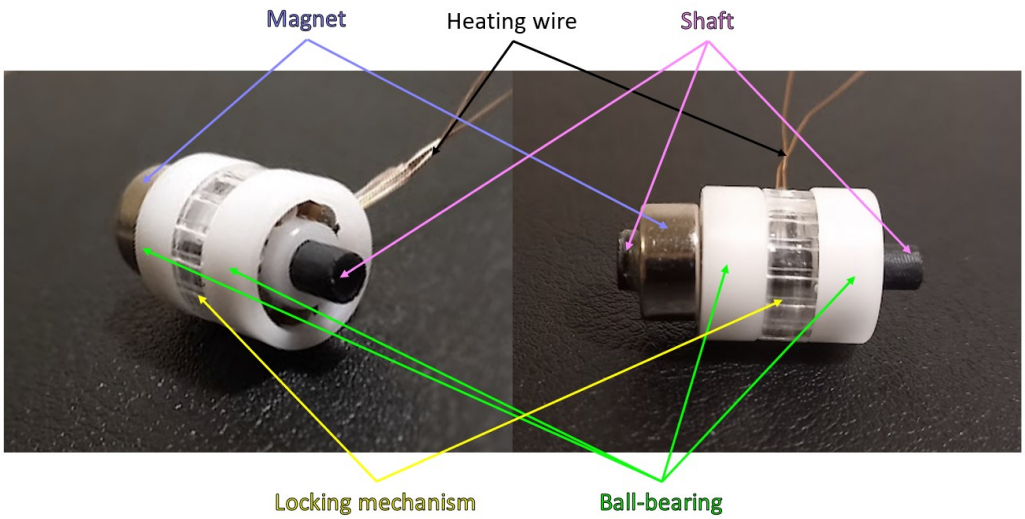

Figure 7: *Final design with magnet, two ball-bearings, shaft, locking mechanism and beam connected to the shaft inside the locking mechanism with heating wires.*

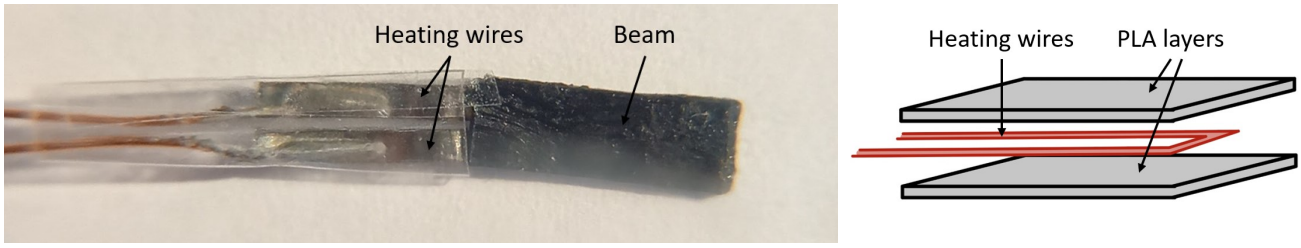

(a) **(b)**

Figure 8: **(a)** *The beam used for the final design with the heating wires coming out of the beam. Tape prevents the two wires from connecting with each other.* **(b)** *The layering of the beam consisting of two thin PLA layers fixed together with a heating wire in between to distribute the heat through the beam.*

Calculating the required dimensions of the beam and force acting on the end of the beam requires some assumptions and requirements. The beam has a length of $L = 2.9$ mm which sticks out of the shaft, and a thickness of $t = 0.5$ mm as determined in Chapter 3.3. The modulus of the beam in a stiff state is determined in by the dynamic mechanical analysis and has a value of $E = 3.87$ MPa. The requirements state that the minimal torque T_{req} the locking mechanism should withstand is $M = 4.0$ Nmm. Figure 9 shows how a torque T in the shaft is compensated by a force F to prevent rotation. The force can be calculated by $F = \frac{T}{L}$. The deflection of the beam in this state is assumed to be almost zero: $y = 0.1$ mm. In this situation according to Equation 12 the required beam width is $w = 2.78$ mm. The width of the beam is therefor chosen to be 3.0 mm.

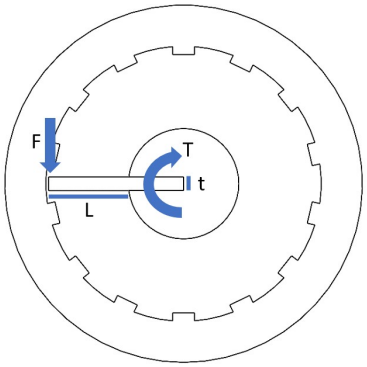

Figure 9: *Schematic drawing of the locking mechanism where a torque T on the shaft results in a compensating force by the locking mechanism on the beam.*

4.3 Thermal characterisation

The PLA beam in this design becomes flexible due to Joule heating. Different currents result in a different maximum temperature of the heating wires and therefor of the beam. Figure 10a shows the influence of different currents on the beam temperature. The temperature increases over time at a constant current until it reaches a maximum temperature. After turning the current off, the temperature decreases again. This figure shows the resulting maximum temperature at currents 0.10, 0.15, 0.20, 0.25 and 0.30 A. The corresponding power can be calculated with Equation 14, 15 and 16 resulting in power outputs of 0.014, 0.031, 0.055, 0.086 and 0.123 W respectively.

The transition temperature of PLA is 64 °C. A current of 0.25 A is chosen for testing the design to match the transition temperature of PLA. The measurement of the heating as a result of the current is stopped just before the temperature stabilizes. The maximum temperature at a current of 0.25 A is approximated at 67 °C. The corresponding elastic storage modulus according to Figure 6 is 50 MPa. Figure 10b shows the temperature distribution after applying a 0.25 A current on the beam.

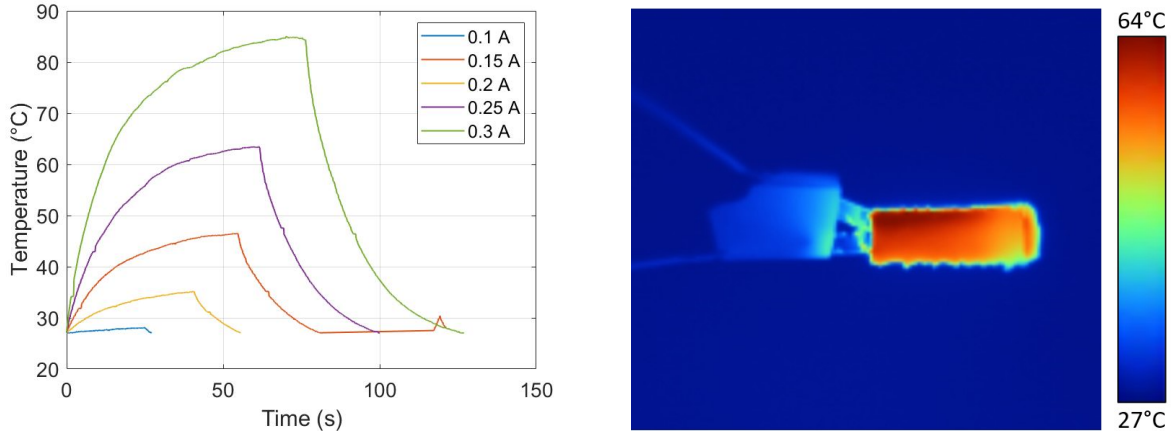

(a) **(b)**

Figure 10: **(a)** *Temperatures of a 0.5 mm thick beam during active Joule heating at different currents. After reaching a maximum, the current is turned off and the beam cools down.* **(b)** *Temperature distribution and the maximum temperature of the 0.5 mm thick beam when heated by heating wires at 0.25 A.*

4.4 Finite Element Analysis

The torque resistance of the locking mechanism is characterised by using PaCMag. First is the magnetic field increased in one direction with the stiff beam to determine what the maximum torque is which the locking mechanism can withstand. The minimal magnetic field the locking mechanism should withstand according to the required 4 Nmm torque is 14.1 mT. Therefore, the magnetic field is increased with steps of 1 mT until 15 mT. This magnetic field of 15 mT corresponds to a torque of 4.2 Nmm by Equation 1 and a force of 1.46 N on the tip of the beam. According to the beam equation 3, this corresponds to a deflection of 0.0983 mm. An FEA of the beam deflection with a mesh size of 0.12 mm when applying a force of 1.46 N is shown in Figure 11a. The FEA gives a deflection of 0.093 mm.

To determine the required torque to rotate the actuated joint (soft beam), the magnetic field in one direction is increased until the flexible beam slips from one dent to the next. At a magnetic field of 3.0 mT (± 0.2) the beam rotates, which corresponds to a torque of 0.859 Nmm and a force of 0.293 N. Since the beam theory only holds for small deflections, is the deflection of the beam in its soft state with a modulus of 50 MPa determined by finite element analysis with mesh size 0.12 mm. Figure 11b shows with a force of 0.293 N on the tip of the beam a deflection 1.333 mm. The deflections for both states of the beam are also given in Table 1.

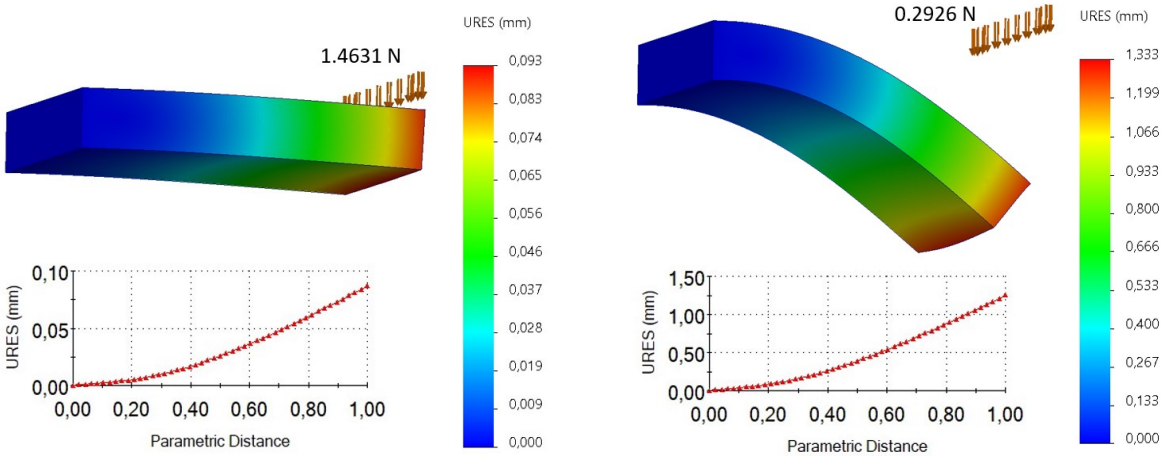

Figure 11: *Finite element analysis of the deflection of the beam with a force acting on one side of the beam. The deflection is shown at its actual scale.* **(a)** *The beam in stiff state with an elastic storage modulus of 3.87 GPa when applying a force of 1.4631 N gives a deflection of 0.093 mm.* **(b)** *The soft beam with an elastic storage modulus of 50 MPa and a force of 0.2926 N on the tip of the beam gives a deflection of 1.333 mm.*

The maximum bending stress σ_{max} in a deflected beam can be calculated with Equation 13 where y_{max} is the distance from the neutral line to the edge of the beam so therefor $y_{max} = \frac{h}{2}$. When a moment on the stiff beam of 4.2 Nmm is applied, is the maximum bending stress at the fixed end of the beam 33.94 N/mm^2. The FEA with mesh size 0.12 mm for the stress in both the stiff and flexible beam is shown in Figure 12. The maximum magnetic field which can be applied on the beam before permanent deformation is 17.7 mT because of the yield strength of 40 MPa. The maximum bending stresses which occurs at the fixed end of the beam are given in Table 1.

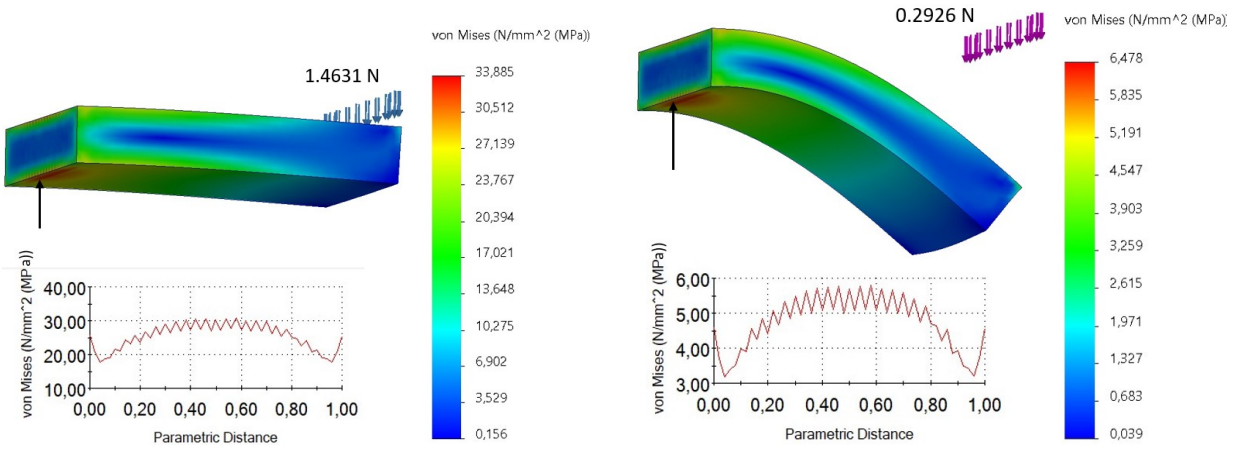

(a) **(b)**

Figure 12: *Finite element analysis results of the bending stress in the beam as a result of a force acting on one side of the beam. The plots show the stress over parametric distance on the edge indicated with the black arrow where the stress in the beam is maximal at the fixed end of the beam.* **(a)** *The stiff beam with a modulus of 3.87 GPa and a force of 1.4631 N on the tip of the beam results in a maximum stress of 33.885 N/mm^2.* **(b)** *The flexible beam with a modulus of 50 MPa and a force of 0.2926 N on the tip of the beam results in a maximum stress of 6.478 N/mm^2.*

Table 1: *For both states of the beam are the deflection and maximum stress determined numerically by the FEA and analytically.*

	Deflection		Maximum Stress	
Modulus	Analytical	Numerical	Analytical	Numerical
3.87 GPa	0.0983 mm	0.093 mm	33.94 N/mm^2	33.885 N/mm^2
50 MPa	-	1.333 mm	-	6.478 N/mm^2

4.5 Backlash

The final design has an outer ring with 14 dents between which the beam is able to lock. The backlash is the rotational freedom the beam has between two dents. By applying a magnetic field in first one direction until the beam hits a dent, and then the in other direction until the beam hits the other dent, determines the backlash of the beam. Figure 13 shows a backlash of 18°of the beam.

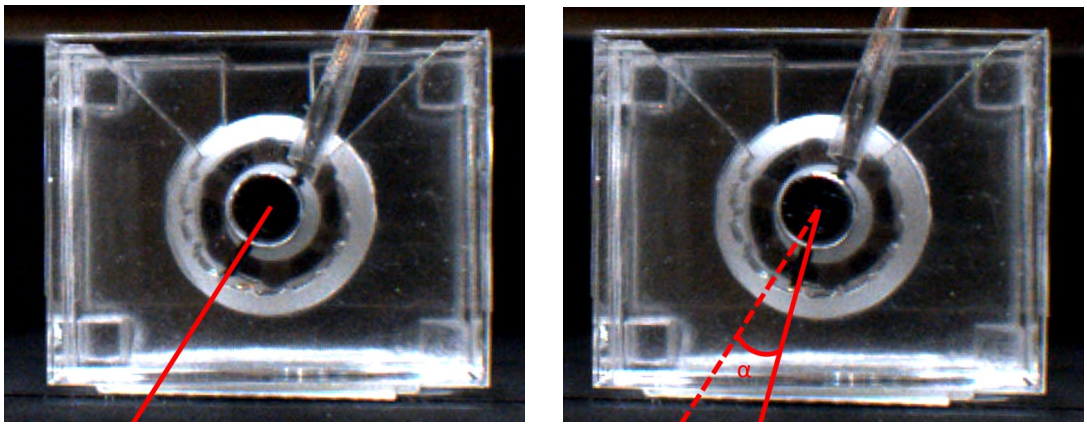

Figure 13: *The backlash of the locking mechanism is equal to 18 °.*

5 Discussion

The locking mechanism designed in this thesis shows that shape-locking and unlocking is possible with a beam made from shape-memory polymer. The SMP has the property of having two states. In the stiff state is the beam able to shape-lock until at least an experimentally tested magnetic field of 15 mT which corresponds to a torque of 4.2 Nmm. This exceeds the required 4.0 Nmm. The deflection of the beam as a result of the torque in the shaft is determined analytically as 0.0983 mm. An FEA gives a deflection of 0.093 mm for the same beam in the same situation which is a 5.4 % lower than the analytically determined value.

The beam in soft state allows rotation of the shaft with respect to the outer housing in two directions. The experimentally tested magnetic field required for rotating from one dent in the locking ring to another dent equals 3 mT ($\pm$ 0.2). This is one fifth of the torque the stiff beam can withstand and corresponds to a torque of 0.8487 Nmm. The deflection in the beam is simulated which gives a value of 1.333 mm. The deflection can not be compared to the deflection determined analytically according to the beam theory, since the beam theory only holds for small deflections.

Aside from the deflection of the beam, also the stress in the beam is determined analytically and numerically via FEA. The maximum stress analytically determined is 33.94 N/mm^2 for the stiff beam, while it has a value of 33.885 N/mm^2 numerically which is 1.4% lower. The yield strength of the PLA beam has a value of 40 MPa which is higher than the maximum stress, therefor the beam should not experience permanent deformation. However since the yield strength is dependent on the PLA color and the pattern in which the 3D printer printed the beam, therefor this yield strength might not be accurate.

Since the maximum stress in the stiff beam is high compared to the yield strength, some adjustments can be made to the design in order to reduce the stress and prevent the beam from permanent deformation. One adjustment is to decrease the beam thickness. This would reduce the stress in the beam, however it would reduce the torque resistance to the third power. To compensate for this, the amount of beams could be increased and therefor distributing the torque over the beams. Increasing the amount of beams could also be used to increase the torque resistance without increasing or decreasing the stress in each beam, since each beam would experience the same deflection and stress. Another adjustment is to make a design where the length of the beam can be increased. This can be done by adjusting the shaft where the beam is connected to. In the design at hand, a straight is shaft used. Adjusting this shaft to have a 'U' shape at the same height as the locking ring where the beam is connected to the valley of the 'U' would leave more space for a longer beam. With an increased length and the same deflection, is the force and therefor the torque in the shaft lower which would result in less stress in the beam. This however also reduces the torque resistance of the locking mechanism.

The torque of the shaft is maximal when the the permanent magnet is perpendicular to the external magnetic field. When testing in the electromagnetic coil setup, the permanent magnet was aligned perpendicular with the axis of the coils being used. Rotating the shaft inside the locking mechanism however, resulted in the magnet getting a different angle and decreasing the torque. All measurements are done with approximately 90 degrees between the field directions of the permanent magnet and the coil configuration. Less than 90 degrees would result in a lower moment as given by Equation 1, smaller force, less stress in the beam and a smaller deflection.

The locking ring of the design has 14 dents and a backlash of 18 °. This makes the design a discrete locking mechanism. In surgical procedures it is required to be able to shape-lock the design at a desired rotation which is not always possible with a discrete locking mechanism. The amount of angles where locking is possible can be increased by increasing the amount of dents in the design. On top of that, two locking

mechanisms can be placed behind each other. One locking ring of 20 dents would create 20 locking positions. Placing two locking rings with 20 dents with an offset would create 40 locking positions. The two locking mechanisms can approximate the desired rotation better than one. Aside from reaching the desired rotation it is also important in surgical procedures that the backlash is minimal. In this design is some rotation still possible because of the backlash of 18 °. Decreasing the space between two dents in the locking ring will decrease the backlash.

For surgical applications the design needs a working channel for surgical instruments. This design does not have a working channel inside the shaft yet because the fabrication method is limited to 3D printing techniques. As a next step, the shaft can be made from non-magnetic metals like aluminum through which a working channel is possible. Aside from surgical instruments, this channel can also be used for the heating wires of the beam. In the current design the wires are sticking out of the design and are not able to rotate infinitely. The electrical connection inside the shaft needs to be redesigned with for example rotary slip rings which keep the electrical connection between a stationary and a rotating part [27].

6 Conclusion

This thesis describes the design of an end-effector with a locking mechanism based on shape-memory polymer. The locking mechanism consists of a beam with dimensions 2.9 $\times$ 3.0 $\times$ 0.5 mm with a heating wire for Joule heating attached to a shaft. The shaft rotates with respect to the outer housing which holds the locking ring consisting of dents and obstructions on which the beam shape-locks in a stiff state. The locking mechanism locks until at least 4.2 Nmm with a deflection of 0.0983 mm and a maximum stress of 33.94 N/mm^2 close to the yield strength of 40 MPa. Joules heating increases the temperature to 64 °C and therefor increases the flexibility in the beam which allows rotation of the shaft with respect to the outer housing. The beam deflects 1.333 mm at a torque of 0.859 Nmm generated by a permanent magnet attached to the tip of the end-effector when an external magnetic field is applied. The design has a discrete locking mechanism where the beam can lock on 14 dents. The shaft has 18 degrees of rotational freedom when the beam is locked in one dent. The design could be improved by increasing the length of the beam and by increasing the amount of beams. To increase the amount of locking positions the amount of dents can be increased and multiple locking mechanisms can be placed behind each other. Decreasing the space between dents decreases the backlash of the design. For surgical applications a locking mechanism closest to continuous locking is desired with a backlash as low as possible.

References

[1] Frederick M. Azar. Minimally invasive surgery: Is less more? *Orthopedic Clinics of North America*, 51(3):xiii–xiv, 2020. ISSN 0030-5898. doi: https://doi.org/10.1016/j.ocl.2020.04.001. URL https://www.sciencedirect.com/science/article/pii/S0030589820300456.

[2] J.L. Ochsner. Minimally invasive surgical procedures. *Ochsner journal*.

[3] T. Williamson and S.E. Song. Robotic surgery techniques to improve traditional laparoscopy. *Journal of the Society of Laparoendoscopic Surgeons*, 2022. doi: https://doi.org/10.4293/JSLS.2022.00002.

[4] J.C. Ngu, C. B. Tsang, and D.C. Koh. The da vinci xi: a review of its capabilities, versatility, and potential role in robotic colorectal surgery. *Robotic surgery*, (4):77–85, 2017. doi: https://doi.org/10.2147/RSRR.S119317.

[5] Lukas Masjosthusmann, Michiel Richter, Pavlo Makushko, Denys Makarov, and Sarthak Misra. Miniaturized variable stiffness gripper locally actuated by magnetic fields. *Advanced Intelligent Systems*, March 2024. doi: 10.1002/aisy.202400037.

[6] Theodosia Lourdes Thomas, Jonathan Bos, Juan J. Huaroto, Venkatasubramanian Kalpathy Venkiteswaran, and Sarthak Misra. A Magnetically Actuated Variable Stiffness Manipulator Based on Deployable Shape Memory Polymer Springs. *Adv. Intell. Syst.*, 6(2):2200465, February 2024. ISSN 2640-4567. doi: 10.1002/aisy.202200465.

[7] Michiel Plooij, Glenn Mathijssen, Pierre Cherelle, Dirk Lefeber, and Bram Vanderborght. Lock your robot: A review of locking devices in robotics. *IEEE Robotics Automation Magazine*, 22(1):106–117, 2015. doi: 10.1109/MRA.2014.2381368.

[8] Bart Peerdeman, Marcello Valori, Dannis Brouwer, Edsko Hekman, Sarthak Misra, and Stefano Stramigioli. Ut hand i: A lock-based underactuated hand prosthesis. *Mechanism and Machine Theory*, 78:307–323, 2014. ISSN 0094-114X. doi: https://doi.org/10.1016/j.mechmachtheory.2014.03.018. URL https://www.sciencedirect.com/science/article/pii/S0094114X14001062.

[9] S Pisani, I Genta, T Modena, R Dorati, M Benazzo, and B Conti. Shape-memory polymers hallmarks and their biomedical applications in the form of nanofibers. *International Journal of Molecular Sciences*, 23(3), Jan 2022. ISSN 1422-0067. doi: 10.3390/ijms23031290. URL https://www.mdpi.com/1422-0067/23/3/1290.

[10] Yang Yang, Yonghua Chen, Yingtian Li, and Michael Zhiqiang Chen. 3d printing of variable stiffness hyper-redundant robotic arm. In *2016 IEEE International Conference on Robotics and Automation (ICRA)*, pages 3871–3877, 2016. doi: 10.1109/ICRA.2016.7487575.

[11] Jinsong Leng, Xin Lan, Yanju Liu, and Shanyi Du. Shape-memory polymers and their composites: Stimulus methods and applications. *Progress in Materials Science*, 56(7):1077–1135, 2011. ISSN 0079-6425. doi: https://doi.org/10.1016/j.pmatsci.2011.03.001. URL https://www.sciencedirect.com/science/article/pii/S0079642511000429.

[12] Tianzhen Liu, Tianyang Zhou, Yongtao Yao, Fenghua Zhang, Liwu Liu, Yanju Liu, and Jinsong Leng. Stimulus methods of multi-functional shape memory polymer nanocomposites: A review. *Composites Part A: Applied Science and Manufacturing*, 100:20–30, 2017. ISSN 1359-835X. doi: https://doi.org/10.1016/j.compositesa.2017.04.022. URL https://www.sciencedirect.com/science/article/pii/S1359835X17301719.

[13] Zheng Tong, Xiaohan Pei, Zejun Shen, Songbo Wei, Yang Gao, Peng Huang, Bairu Shi, Fuchao Sun, and Tao Fu. An enhanced thermo-actuated shape memory polymer composite coupled with elastomer. *Pet. Explor. Dev.*, 43(6):1097–1106, December 2016. ISSN 1876-3804. doi: 10.1016/S1876-3804(16)30128-8.

[14] Mariana Cristea, Daniela Ionita, and Manuela Maria Iftime. Dynamic Mechanical Analysis Investigations of PLA-Based Renewable Materials: How Are They Useful? *Materials*, 13(22), November 2020. doi: 10.3390/ma13225302.

[15] Introduction to Dynamic Mechanical Analysis and its Application to Testing of Polymer Solids - TA Instruments, jul 2024. URL https://www.tainstruments.com/applications-notes/introduction-to-dynamic-mechanical-analysis-and-its-application-to-testing-of-polymer-soli [Online; accessed 30. Jun. 2024].

[16] Ken Gall, Martin L. Dunn, Yiping Liu, Dudley Finch, and Naseem A. Munshi. Shape Memory Polymer Nanocomposites. *Acta Mater.*, 50(20):5115–5126, December 2002. ISSN 1359-6454. doi: 10.1016/S1359-6454(02)00368-3.

[17] (DMA) Dynamic Mechanical Analysis: Tension, Torsion, Compression, February 2023. URL https://www.rheologylab.com/services/dynamic-mechanical-analysis-dma. [Online; accessed 31. May 2024].

[18] María Martínez Gomez. Permanent Magnets. In *Encyclopedia of Electrical and Electronic Power Engineering*, pages 219–228. Elsevier, Walthm, MA, USA, January 2023. ISBN 978-0-12-823211-8. doi: 10.1016/B978-0-12-821204-2.00124-0.

[19] Simone Schürle, Bradley E. Kratochvil, Salvador Pané, Mohammad Arif Zeeshan, and Bradley J. Nelson. *Generating Magnetic Fields for Controlling Nanorobots in Medical Applications*. January 2013. ISBN 978-1-4614-2118-4. doi: 10.1007/978-1-4614-2119-1_14.

[20] Ferdinand P. Beer, E. Russell Johnston Jr., John T. DeWolf, and David F. Mazurek. *Statics and Mechanics of Materials*. McGraw-Hill, 2009.

[21] J.P. Holman. *Heat transfer*. McGraw-Hill Book Company, 6th edition. URL https://sv.20file.org/up1/412_0.pdf.

[22] Dezhi Song, Shuxin Wang, Zhiqiang Zhang, Xiangyang Yu, and Chaoyang Shi. A Novel Continuum Overtube With Improved Triangulation for Flexible Robotic Endoscopy. *IEEE Transactions on Medical Robotics and Bionics*, 5(3):657–668, July 2023. ISSN 2576-3202. doi: 10.1109/TMRB.2023.3294527.

[23] Neodymium Magnets (NdFeB) | Arnold Magnetic Technologies, July 2021. URL https://www.arnoldmagnetics.com/products/neodymium-iron-boron-magnets. [Online; accessed 23. Jun. 2024].

[24] Reely Kugellager Kunststoff Innen-Durchmesser: 4 mm Außen-Durchmesser: 13 mm, June 2024. URL https://www.conrad.de/de/p/reely-kugellager-kunststoff-innen-durchmesser-4-mm-aussen-durchmesser-13-mm-236052.html. [Online; accessed 27. Jun. 2024].

[25] Adi Pandžić, Damir Hodzic, and Aleksa Milovanović. *Effect of Infill Type and Density on Tensile Properties of PLA Material for FDM Process*. October 2019. ISBN 978-3-90273422-8. doi: 10.2507/30th.daaam.proceedings.074.

[26] Stainless Steel - Austenitic - 1.4301 (304) Bar and Section, June 2024. URL https://www.aalco.co.uk/datasheets/Stainless-Steel-14301-304-Bar-and-Section_34.ashx. [Online; accessed 27. Jun. 2024].

[27] Rotary slip ring connectors — what are they used for? , July 2024. URL https://www.connectortips.com/rotary-slip-ring-connectors-what-are-they-used-for-faq. [Online; accessed 30. Jun. 2024].

7 Appendix

A Concepts

The first concepts for a locking mechanism made for this thesis are described in this section. These designs consist of an outer ring and an inner ring made from PMMA. The SMP used here is Norland Optical Adhesive 63 (NOA63). The adhesive can be molded and cured under long wavelenght UV-light under specific temperatures which will approximate transition temperature.

The first concept can be seen in Figure 14. The outer ring and shaft (not shown) rotate with respect to each other when the locking mechanism is unlocked. The SMP fills the entire space in between locking ring and shaft. When the SMP is stiff, no rotation is possible. When the SMP becomes flexible, rotation should be possible, however the required torque needed is really high because of the depth of the dents. This design also has discrete locking instead of continuous locking due to only being able to lock when the shape of the SMP and outer ring coincide.The high volume of SMP requires more time and a high current to heat the volume so rotation is possible.

The second concept also shown in Figure 14 is a variation on the first concept, also consisting of a solid high volume SMP shape interacting with the hills on the surface of the outer ring. This design however uses a circular SMP shape with larger diameter compared to the hills of the outer ring. The SMP therefor shape-locks on the dents when the SMP is in the glassy state. When heated, the SMP dents in at a different place. This concept is continuous, however the distinction between friction-based locking and mechanical shape-locking is hard. The design is based on trial and error for the diameters of the SMP and outer ring. This is in order to have a locking mechanism to withstand 4 Nmm while the SMP is glassy, but can rotate when the SMP is rubber-like.

The third design has a thin ring of SMP which shape-locks in the dents of the locking ring. When the SMP is heated above the transition temperature, the SMP becomes flexible so rotation to a next dent is possible. This design is, similar to the first concept, a discrete locking mechanism. The design is also hard to connect to the theory which makes the design not reconfigurable.

The fourth design shown in Figure 14 is the concept of the design elaborated in this thesis. The design consists of a beam shape-locking on dents on the locking-ring. The shape and deflection of the beam and the stresses inside the beam can be calculated using the beam theory. This design is also reconfigurable. Since connecting the design to the theory has a higher priority compared to designing a continuous locking mechanism, this design is chosen for testing and experimenting. PLA instead of NOA63 is used in this thesis since the NOA63 showed brittle behaviour for large deflections and heating.

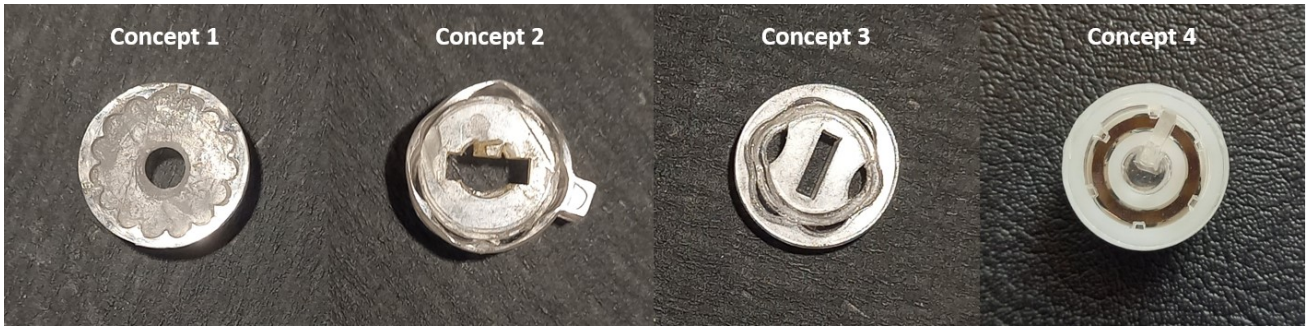

Figure 14: *Four concepts designed for this thesis. The fourth concepts is elaborated in the main text of this thesis.*